THE KINETICS OF THERMAL DECOMPOSITION AND HOT-STAGE MICROSCOPY OF SELECTED ENERGETIC COCRYSTALS

by

Joshua T. Dean

A Thesis

Submitted to the Faculty of Purdue University

In Partial Fulfillment of the Requirements for the degree of

Master of Science in Mechanical Engineering

School of Mechanical Engineering

West Lafayette, Indiana

May 2020

THE PURDUE UNIVERSITY GRADUATE SCHOOL
STATEMENT OF COMMITTEE APPROVAL

Dr. Steven F. Son, Chair

School of Mechanical Engineering

Dr. Metin Örnek, Co-Chair

School of Aeronautics and Astronautics

Dr. Davin Piercey

School of Aeronautics and Astronautics

Approved by:

Dr. Steven F. Son

Dedicated to my God, my family, and my friends who made this possible.

ACKNOWLEDGMENTS

This research was sponsored by and was accomplished under the Army Research Office Multidisciplinary University Research Initiative Grant # W911NF-13-1-0387. Additionally, the author acknowledges the Matzger Research Group at the University of Michigan and Picatinny Arsenal for providing cocrystal samples.

The author would also like to acknowledge Dr. Metin Örnek, Tim Manship, and Dr. Steven Son for the countless hours they spent providing guidance, teaching me, and revising this thesis.

TABLE OF CONTENTS

LIST OF TABLES

LIST OF FIGURES

ABSTRACT

The thermal decomposition of four energetic cocrystals composed of 4-amino-3,5-dinitropyrazole (ADNP)/diaminofurazan (DAF), 2,4,6-trinitrotoluene (TNT)/ 2,4,6,8,10,12-hexanitro-2,4,6,8,10,12-hexaazaisowurtzitane (CL20), 1,3,5,7-tetranitro-1,3,5,7-tetrazacyclooctane (HMX)/CL20, and 1-methyl-3,5-dinitro-1,2,4-triazole (MDNT)/CL20 were studied using simultaneous differential scanning calorimetry (DSC), thermogravimetry analysis (TGA), and hot-stage microscopy. The kinetic parameters of their thermal decomposition reaction were determined using the Kissinger and Ozawa kinetic analysis methods. Each cocrystal's peak exothermic temperature (decomposition temperature), activation energy, and pre-exponential constant are reported. Furthermore, these parameters from each cocrystal were compared to the same parameters from the corresponding stoichiometric physical mixture in order to identify changes in behavior attributable to the cocrystallization process. For ADNP/DAF, the cocrystal shows an 8% increase in the peak exotherm temperature and a 11-13% decrease in peak activation energy as compared to its physical mixture. For TNT/CL20, this comparison shows a much smaller change in the peak exotherm temperature (<1%) but shows a 5% decrease in activation energy. This cocrystal also experiences phase stabilization—where a phase transition of one or both coformers is omitted from the decomposition process. The HMX/CL20 cocrystal shows a 1% change in the peak exotherm temperature and shows a 2% increase in activation energy. Finally, for MDNT/CL20, this comparison shows nearly a 4% increase and a drastic decrease in peak activation energy by 42-44%. Cocrystallization clearly affects the thermal decomposition and reaction kinetics of these materials, offering the potential to create a hybrid-class of energetic materials which combines the high performance of an energetic material with the safety and insensitivity of another.

Keywords: Energetic cocrystal; Thermal decomposition; Kinetics analysis; Kissinger method; Ozawa method; Hot-stage microscopy.

1. INTRODUCTION

Energetic materials are commonly used in explosives, propellants, and pyrotechnics across an array of applications ranging from civilian to military and from subsurface to space. These materials are utilized in this manner due to their stored chemical energy, which can be released through heat or impact (Landenberger and Matzger 2010; Liu et al. 2016; J. Zhang and Shreeve 2016). The optimization of performance and safety of the energetic materials have been the subject of study for centuries and remains one of the prevalent motivations behind energetic material research currently. One of the preeminent safety concerns with the usage, storage, and transportation of energetic materials is thermal runaway, colloquially known as "cook-off"(Rogers 1975; Dickson, P.M., Asay, B.W., Henson, B.F., Smilowitz 2004). Cook-off occurs when an energetic material's thermal decomposition becomes self-sustaining, leading to an explosion of the material. There have been numerous cook-off incidents throughout history where the explosion of the material has caused catastrophic damage and loss of life, such as the Texas City disaster in 1947 (Cunningham 2019) and the *USS Forrestal* fire in 1967 (Cox 2005). The risk of cook-off can be greatly reduced through the knowledge of the material's thermal behavior. Parameters such as activation energy, pre-exponential constant, melting temperature, and decomposition temperature, allow for the characterization of the material's thermal behavior; in turn, this characterization assists in the determination of usage, storage, and transportation methods of a specific energetic material (J. Q. Zhang et al. 2018; Jia et al. 2019).

Cocrystallization, in contrast to its longstanding use in the pharmaceutical industry, has recently been adopted to energetic materials (Landenberger and Matzger 2010; 2012; Vuppuluri et al. 2018; J. Zhang and Shreeve 2016). The intent behind this is two-fold: it is cost-effective and holds the potential to create hybrid materials with desired behavior and properties. Rather than dedicating significant time into developing and characterizing new molecules, cocrystals are mixtures of two or more types of known molecules, known as coformers, with a unique crystal arrangement held by weak intermolecular forces (Landenberger and Matzger 2010; J. Zhang and Shreeve 2016). Because of this unique crystal arrangement, the cocrystal has the propensity to possess mechanical, thermal, or chemical properties which differ from its coformers. Through cocrystallization, researchers seek to improve both the safety and performance of energetic

materials beyond the limits of current energetic materials or their physical mixtures (Yang et al. 2012). Since cocrystallization is relatively new to the field of energetic materials, the nature of energetic cocrystals remains largely uncharacterized.

4-amino-3,5-dinitropyrazole (ADNP or LLM-116) is an important energetic material that has a high detonation performance and low sensitivity to impact ($h_{50\%}$ = 167.5cm) (Schmidt et al. 2001) and friction (Wang et al. 2014), but it suffers from a poor thermal sensitivity and decomposes around 180 °C (Bennion, Siddiqi, and Matzger 2017). 3,4-diaminofurazan (DAF) is a high-nitrogen material which possesses a low density (1.61g/cm^3) and an oxygen balance (%OB = -80) like TNT (Bennion, Siddiqi, and Matzger 2017; Y. Li et al. 2016). An energetic cocrystal was formed from ADNP and DAF by the Matzger Research Group at the University of Michigan (Bennion, Siddiqi, and Matzger 2017).

2,4,6-trinitrotoluene, more commonly known as TNT, is one of the most common and widely used explosive in existence today due to its insensitivity and moderate performance. TNT also has the ability to be melted down and cast into specific geometries (melt-castable). While 2,4,6,8,10,12-hexanitro-2,4,6,8,10,12-hexaazaisowurtzitane (also known as HNIW or CL20) is currently one of the most powerful explosives in existence (Anderson et al. 2016) and has a high density (1.95-2.08 g/cm^3) (Bolton and Matzger 2011) and good oxygen balance (-10.95%), it suffers from high mechanical sensitivity ($h_{50\%}$ = 29 cm) (Bolton et al. 2012). TNT/CL20 were combined in a cocrystal with the hopes of achieving a melt-castable energetic cocrystal with the safety and insensitivity of TNT while maintaining the performance of CL20 (Bolton and Matzger 2011; X. Li et al. 2017).

1,3,5,7-tetranitro-1,3,5,7-tetrazacyclooctane (HMX) is a common high explosive used in military applications and ordnance due to its higher detonation velocity (9,384 m/s) and good sensitivity to heat and impact ($h_{50\%}$ = 55 cm) (Bolton et al. 2012; Landenberger and Matzger 2012; Sabatini and Oyler 2015). HMX/CL20 were combined in a cocrystal for similar reasons; maintaining the safety and reliability of HMX while achieving the power of CL20 (Bolton et al. 2012; Gao et al. 2014).

1-methyl-3,5-dinitro-1,2,4-triazole (MDNT) possesses higher explosive performance due to its high density (1.67 g/cm^3) and has been identified as a potential candidate to replace TNT in a melt-castable cocrystal (Anderson et al. 2016). Anderson et al. synthesized a MDNT/CL20 cocrystal in 1:1 molar ratio through resonant acoustic mixing which displayed less sensitivity to

friction than CL20 while possessing similar impact and ESD sensitivity (2016). Vuppuluri et al. found the detonation velocity of the MDNT/CL20 cocrystal to be 600m/s faster than that of HMX and attributed the observed difference in detonation velocity between the MDNT/CL20 cocrystal and physical mixture to the cocrystal's unique structure (2018).

Previous studies focused on these cocrystals have identified some of the thermal behavior parameters, such as melting point and decomposition point, but few have delved into an analysis of the cocrystal's reaction kinetics. In this study, the thermal decomposition of four energetic cocrystals made of ADNP/DAF, TNT/CL20, HMX/CL20, and MDNT/CL20 were studied and compared to their corresponding stoichiometric physical mixtures using differential scanning calorimetry (DSC), thermogravimetric analysis (TGA), and hot-stage microscopy. The kinetic parameters of the thermal decomposition were obtained from kinetic analysis using Kissinger and Ozawa methods. The peak endothermic and exothermic temperatures, along with the corresponding activation energies and pre-exponential constants, are reported. Finally, the parameters found from the energetic cocrystals are compared to their respective stoichiometric physical mixture to assess differences attributable to cocrystallization.

2. MATERIALS AND METHODS

2.1 Cocrystals and Coformers

The ADNP/DAF cocrystal and ADNP powders used in this study were provided by the Matzger Research Group at the University of Michigan. A detailed synthesis procedure and analytical characterization studies of ADNP/DAF cocrystal can be found elsewhere (Bennion, Siddiqi, and Matzger 2017). The ADNP used in this study was verified to have purity in excess of 99% through nuclear magnetic resonance (NMR) spectroscopy (Bennion, Siddiqi, and Matzger 2017). The DAF used in this study was purchased from Sigma Aldrich (97% purity).

The TNT/CL20 cocrystal used in this study was synthesized at Purdue University following the methods by Bolton and Matzger (2011) and was verified to have purity of 85% through powder x-ray diffractometry. Briefly, the requisite amounts of TNT and CL20 with a proper molar ratio was measured and placed into a vial containing ethanol. The vial was then placed on an orbital shaker and was agitated for four days until crystals were observed to form from the suspension. The formed cocrystals were then collected through a filter paper. The HMX/CL20 and MDNT/CL20 cocrystals along with CL20 and MDNT powders used in this study were provided by Picatinny Arsenal. The HMX used in this study was Grade B HMX purchased from BAE Systems.

2.2 Preparation of Physical Mixtures

Two different methods were used to prepare a physical mixture in this study. In the first method, which was used to prepare the physical mixtures of ADNP/DAF and HMX/CL20, two coformers were added to a vial and then placed on a roller mill. The vial was rotated for 30 minutes to ensure thorough mixing of the coformer powders. In the second method, the physical mixtures of TNT/CL20 and MDNT/CL20 were prepared through the use of a hexane suspension. The coformer material was added to a vial and physically shaken for 30 seconds to initially intermix the materials. Following this, 30 milliliters of hexane was added to the vial; the vial was then physically shaken again for 30 seconds. The vial containing the materials suspended in hexane were added to an ultrasonic water bath and ultrasonically agitated for five minutes. The

suspension was then poured from the vial into an evaporating dish and the hexane was allowed to evaporate. Once all of the hexane had evaporated, the material was collected and placed into a separate vial for storage.

2.3 Characterization

Particle analysis studies were conducted to quantify the size distribution and general shape of the cocrystal particles using a Malvern Morphologi G3-ID morphologically-directed Raman spectroscopy. The particle size of the studied materials is vital since it plays a significant role in the thermal decomposition behavior of a material, both in bulk and as individual particles(Fathollahi, Pourmortazavi, and Hosseini 2008). In a study by Fathollahi, Pourmortazavi, and Hosseini, decreases in particle size reduced the peak decomposition temperature and the kinetic parameters of HMX used in the study (2008). While not a main point of investigation within this study, particle size analysis was conducted to serve as a frame of reference for comparison with future studies.

The thermal decomposition of the aforementioned materials studied using simultaneous differential scanning calorimetry (DSC) and thermogravimetric analysis (TGA). A TA Instrument SDT Q600 instrument was used to analyze the cocrystals, their physical mixtures, and their coformers under the following test conditions: heating rates of 15, 10, 5, and 2 °C per minute; temperature range from 25 to 350°C; sample masses ranging from 1 to 2 milligrams; using open alumina sample pans; and an argon (99.999% purity) purge with a flow rate of 100 milliliters per minute. The smaller sample sizes were chosen to mitigate risk of thermal runaway within the sample and to allow greater resolution on thermal events if occurring in close proximity (Banerjee 1993). The open alumina pans were used in lieu of sealed/hermetic pans to enable the use of a mass spectrometer (MS) in conjunction with the DSC/TGA for analysis and publication in subsequent studies.

Hot-stage microscopy studies were conducted to visually observe and characterize the events identified during the DSC/TGA studies using a Linkam T1000 hot-stage. Sample were placed onto a 5-millimeter sapphire window and enclosed with a 6-millimeter disc of Kapton tape. It is worth to note sample masses were significantly smaller in order to increase the ability to observe individual particles. The Kapton tape was selected to reduce particle movement

during heating and for its tolerance to heating. Samples were heated from 25 to 350°C at a heating rate of 15 °C per minute with no gas purging.

2.4 Kinetic Analysis

Using the data produced from the DSC/TGA studies, the chemical reaction kinetics were analyzed using the Kissinger and Ozawa methods. Kissinger's method is shown in Eq. 1 as below;

$$\ln\left(\frac{\beta}{T_p^2}\right) = \ln\left(\frac{AR}{E_a}\right) - \frac{E_a}{R}\left(\frac{1}{T_p}\right) \quad (1)$$

where β is the heating rate, T_p is the peak temperature of the sample's exotherm, R is the universal gas constant (8.314 Joules/mole-Kelvin), A is the pre-exponential constant, and E_a is the activation energy (Blaine and Kissinger 2012). Using the values of $\ln\left(\frac{\beta}{T_p^2}\right)$ as a function of $\frac{1}{T_p}$ produces a straight line, whose slope could be used to calculate the activation energy of the sample, and the y-intercept of the trendline provides the pre-exponential constant (Blaine and Kissinger 2012).

A similar approach is found with Ozawa's isoconversional method of determining kinetic parameters as shown in Eq. 2 below (Fathollahi, Pourmortazavi, and Hosseini 2008; Sis 2009).

$$\ln(\beta) = \left(\ln\left(\frac{AE_a}{R}\right) - 5.331\right) - \frac{1.052E_a}{R}\left(\frac{1}{T_p}\right) \quad (2)$$

The conversion extent is assumed to be constant, which reduces the reaction rate to a function of temperature only. The equation varies slightly in comparison to Kissinger method due to the incorporation of Doyle's approximation (Doyle 1962); however, still uses the peak temperature of the sample's exotherm to create a plot with the values of $\ln(\beta)$ as a function of $\frac{1}{T_p}$ produces a straight line. The slope of this line provides the peak activation energy of the sample, and the y-intercept of the trendline provides the pre-exponential constant (Fathollahi, Pourmortazavi, and Hosseini 2008; Sis 2009).

3. RESULTS AND DISCUSSION

3.1 Powder Morphology and Size

The cocrystals were initially imaged under the digital microscope to observe their morphology (Fig. 3.1) and a particle size analysis was performed to gain an understanding of the particle size (Table 3.1).

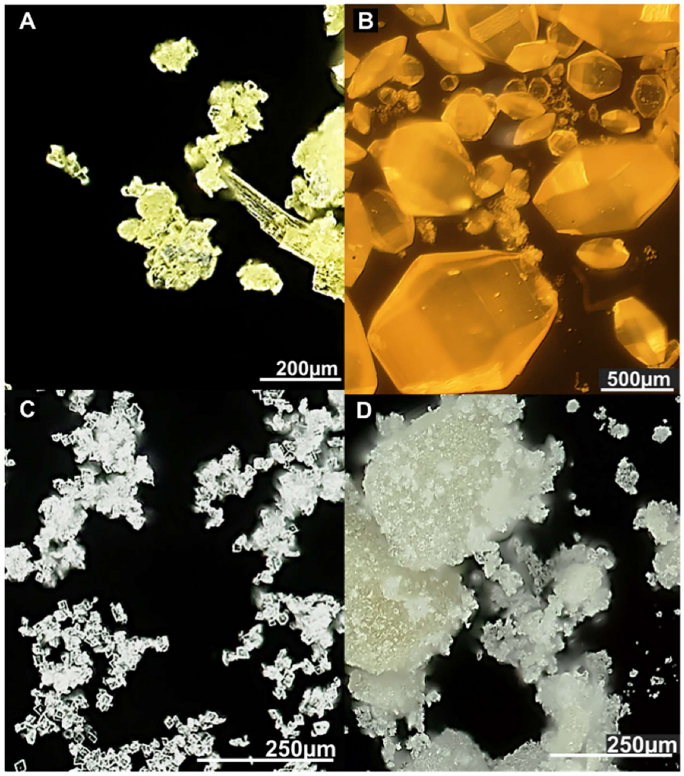

Fig. 3.1. Digital microscope images of **a)** ADNP/DAF **b)** TNT/CL20 **c)** HMX/CL20 and **d)** MDNT/CL20 cocrystal samples.

ADNP/DAF cocrystal particles are generally rod-shaped and yellow in color as seen in Fig. 3.1a. Despite their color, they are generally transparent. The individual particles display a tendency to conglomerate and are brittle, suggesting a particle size distribution might be skewed towards finer, smaller individual particles and larger agglomerates. The TNT/CL20 particles resemble the morphology displayed by ε-phase CL20 particles (Zhu et al. 2015), looking like elongated gemstones with cut facets on all sides (Fig. 3.1b). This cocrystal is unique in that the morphology is maintained regardless of particle size and do not display the tendency to

conglomerate. The particles are yellow when viewed through a microscope but a sample of TNT/CL20 powder appears as a light orange color. This contradicts the findings of Bolton and Matzger, who found the TNT/CL20 cocrystal to be colorless (2011). However, this discrepancy can easily be attributed to the lower purity of the TNT/CL20 cocrystal in this study. Particles are not opaque and present the appearance of lightly frosted glass.

HMX/CL20 appears as a rectangular prism, clear in color and generally transparent (Fig. 3.1c). In bulk powder, HMX/CL20 is white and has the consistency of powdered sugar. HMX/CL20 powder is very cohesive and the individual particles tend to form agglomerates. From visual observation, the particle size distribution appears to be nearly uniform. MDNT/CL20 particles appear generally white or beige in color; however, MDNT/CL20 bulk powder is yellow in color (Fig. 3.1d). The particles are irregular in shape and texture, but the shape generally trends towards an oval or ellipsis. The particles tend to form very large agglomerates and only appear as individual particles when dislodged from the agglomerates.

Table 3.1. Particle size analysis data for the cocrystal powders.

Parameter	ADNP/DAF	TNT/CL20	HMX/CL20	MDNT/CL20
Mean Diameter (μm)	16.62	22.48	11.20	6.57
D_{90} Diameter(μm)	35.73	33.71	20.47	0.54
Maximum Diameter (μm)	136.21	1,052.58	113.43	179.96
Standard Deviation (μm)	14.56	48.75	7.44	6.99
Aspect Ratio	0.659	0.671	0.661	0.693

If the four cocrystals studied were arrayed on a spectrum of mean diameter, ADNP/DAF cocrystal would fall near the middle of that spectrum. The aspect ratio mean supports the initial observation of rod-shaped particles and coincides with the literature (Bennion, Siddiqi, and Matzger 2017). On a spectrum of mean diameter for the four cocrystals studied, TNT/CL20 is the largest. TNT/CL20 also had some of the largest particles observed, in excess of one millimeter in diameter. The aspect ratio mean supports the “elongated gemstone” observation made under the microscope. Referring back to the spectrum of mean diameter for the cocrystals studied, HMX/CL20 would fall near the middle. The aspect ratio mean supports the conclusion that HMX/CL20 cocrystal particles are generally rectangular in nature.

The MDNT/CL20 particles are the smallest particles observed in this study. The aspect ratio mean supports the qualitative assessment previously stated, with MDNT/CL20 particles generally assuming an oblong shape.

3.2 Thermal Analysis

3.2.1 ADNP/DAF

The DSC/TGA traces of the cocrystal, the stoichiometric physical mixture, and their respective peak exothermic temperatures are as shown in Fig. 3.2.

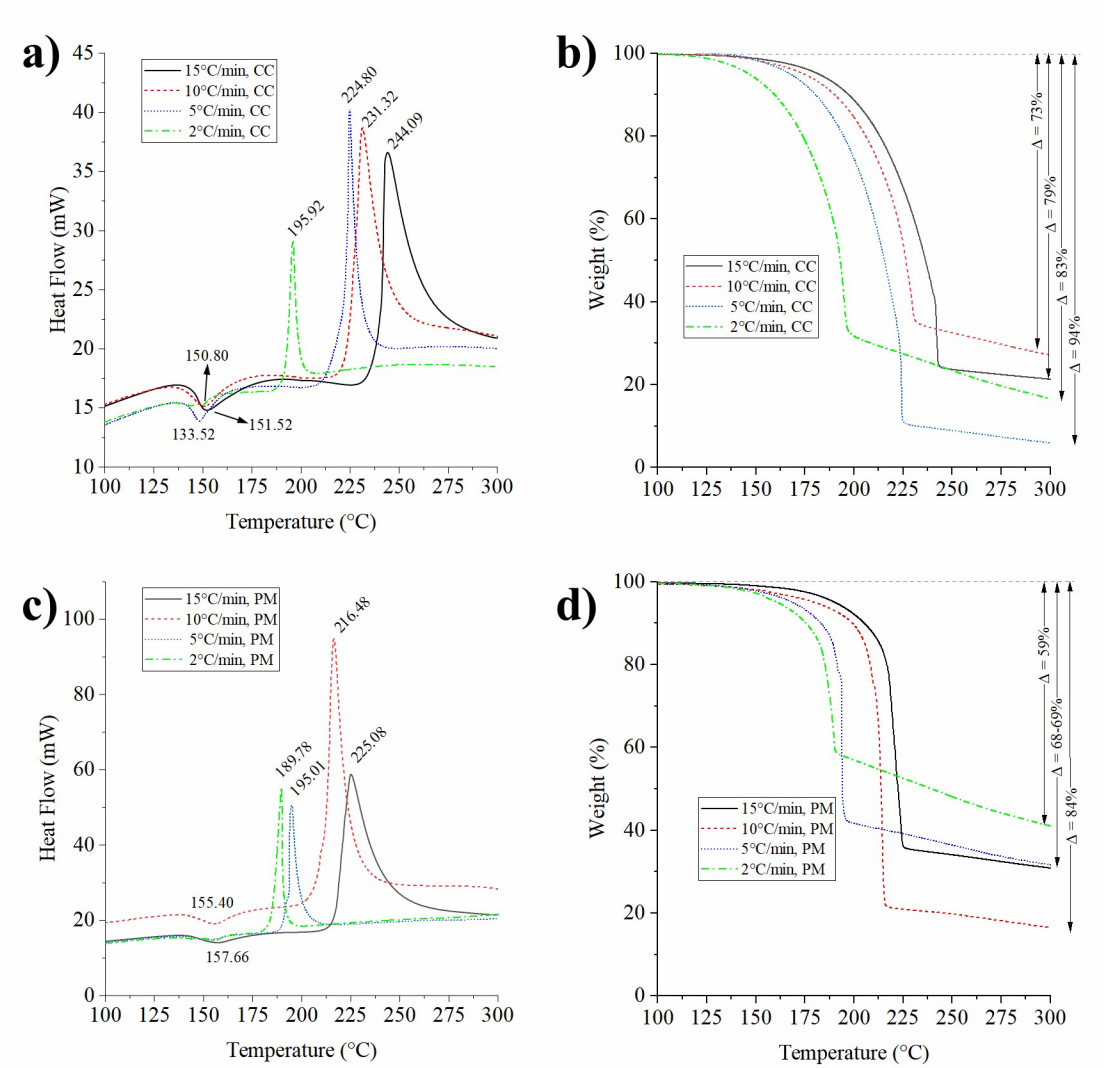

Fig. 3.2. DSC and TGA traces of **(a-b)** ADNP/DAF cocrystal and **(c-d)**ADNP/DAF physical mixture at varying heating rates in open pan. CC and PM as shown in plot legend refer to cocrystal and physical mixture, respectively.

Decomposition is a kinetic phenomenon—it is dependent on both time and temperature. At higher heating rates, the decomposition reaction achieves a higher temperature in the time it takes the reaction to proceed to completion. Exothermic peak temperatures shift to the right as the heating rates increase for all the samples (Fig. 3.2a and 3.2c). Despite the similarity in their thermal behavior as described by the DSC data, the cocrystal shows a slightly lower melting point than the physical mixture while maintaining a higher decomposition temperature than the physical mixture. This is ideal for a melt-castable cocrystal, which was the intent behind its development. The cocrystal also demonstrates a eutectic melting point, and a higher decomposition temperature than ADNP (Table 3.2).

The ADNP/DAF cocrystal and the physical mixture both display single-stage decomposition as evidenced by their respective TGA plots, which bear a remarkable resemblance to each other (Fig. 3.2b and 3.2d). This comes as no surprise since Bennion, Siddiqi, and Matzger found the ADNP/DAF cocrystal can be synthesized from melting the ADNP/DAF stoichiometric physical mixture (2017).

Table 3.2. Comparison of peak DSC temperatures for ADNP/DAF cocrystal, physical mixture, and individual coformers at a 15 °C/min heating rate.

Material	Cocrystal	Physical Mixture	ADNP	DAF
Peak Endotherm Temperature (°C)	151.5	157.7	175.4	181.1
2nd Endotherm Temperature (°C)	--	--	--	247.2
Peak Exotherm Temperature (°C)	244.1	225.1	183.2	--

Hot-stage microscopy was performed on the ADNP/DAF cocrystal and several images were taken while the sample was heated to elevated temperatures. Figure 3.3 shows the images of ADNP/DAF cocrystals taken during heating. A baseline image was also included as can be seen in Fig. 3.3a. Bubbles formed and were observed moving within the individual particles at approximately 110°C, and particle movement was observed at approximately 120°C. The particles became optically thick prior to melting; melting onset occurred between 145-150°C (Fig. 3.3b). This corroborates our findings from the DSC/TGA studies and further concurs with the results found in the literature (Bennion, Siddiqi, and Matzger 2017). Particles appear to agglomerate as they melt, reducing to a large pool of liquid material upon completion of the melt (Fig. 3.3c and 3.3d). The arrows shown in Fig. 3.3d identify the direction of travel for the molten

material as it spread across the observation area. At approximately 190°C, the liquid occupying the observation area begins to recede (Fig. 3.3e). The arrows in Fig. 3.3e and 3.3f, as well as the dashed line placed for comparison, show the direction and extent of the liquid's retrograde from the observation area. This indicates vaporization of the liquid material is taking place.

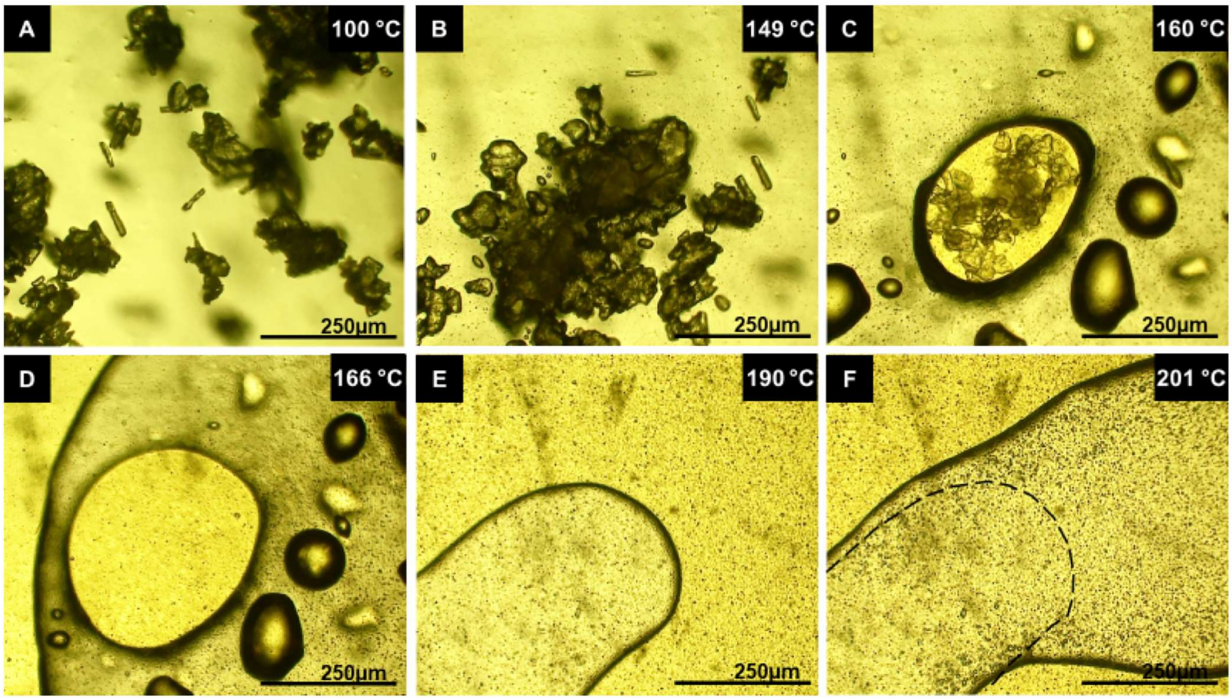

Fig. 3.3. Hot-stage microscopy images of ADNP/DAF cocrystal sample at **a)** 100°C, **b)** 149°C, **c)** 160°C, **d)** 166°C, **e)** 190°C, and **f)** 201°C.

3.2.2 TNT/CL20

DSC/TGA traces for the TNT/CL20 cocrystal and physical mixture are shown in Fig. 3.4. The melting peak temperature ranges from approximately 135-144°C across all heating rates. This is the first cocrystal in the study which experiences phase stabilization; the 80°C endotherm caused by TNT melting is no longer apparent. The peak exothermic temperatures resulting from the decomposition of the cocrystal range from 231-257°C and increase with higher heating rates as expected due to reaction kinetics (Fig. 3.4a and 3.4c).

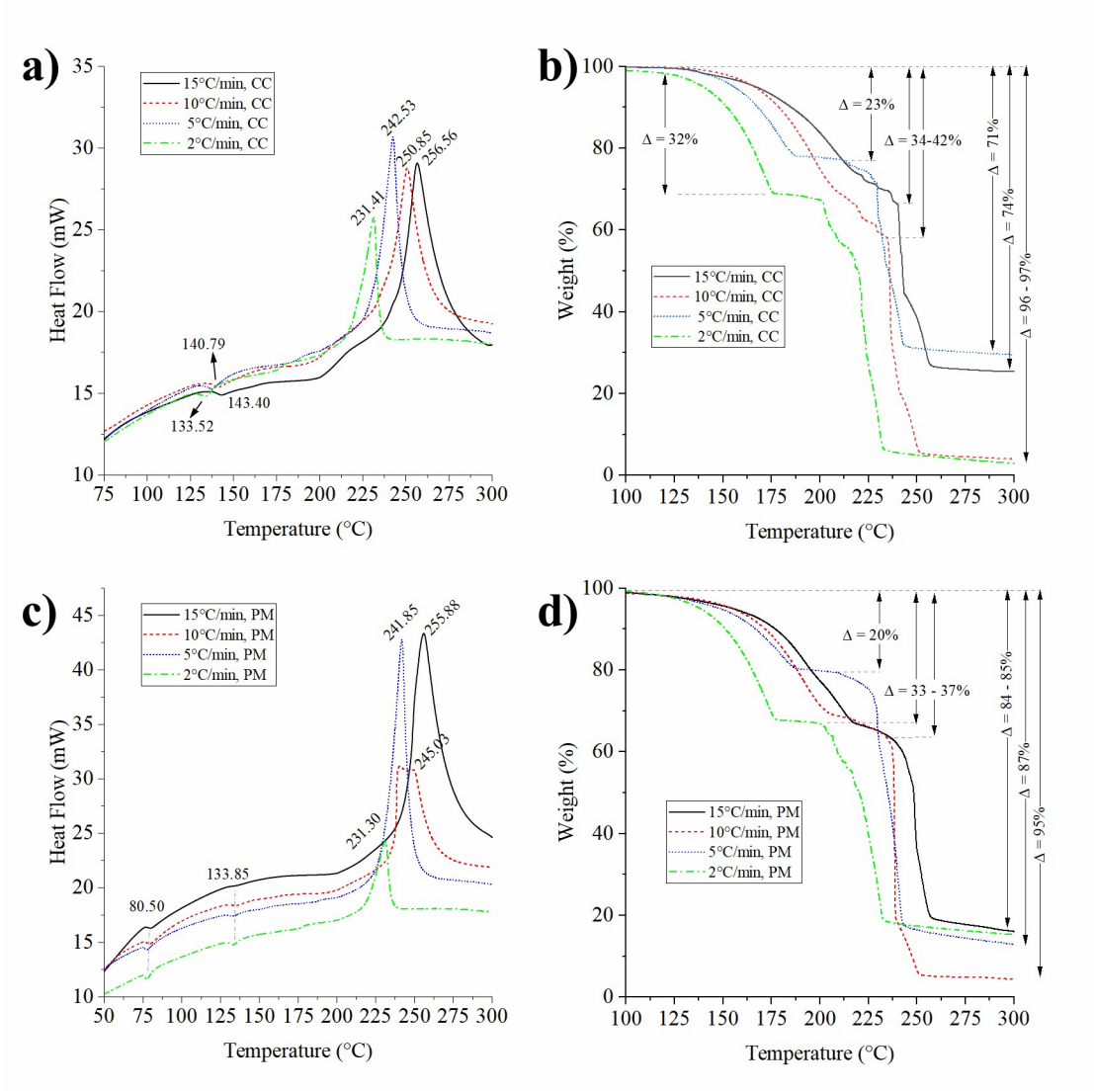

Fig. 3.4. DSC and TGA traces of **(a-b)** TNT/CL20 cocrystal and **(c-d)** TNT/CL20 physical mixture at varying heating rates in open pan. CC and PM as shown in plot legend refer to cocrystal and physical mixture, respectively.

The physical mixture experiences an endotherm at 80°C, and another endotherm at approximately 130°C (Fig. 3.4c). The endotherm observed at 80°C and lack of mass loss suggests the melt of a coformer, likely TNT. The endotherm observed at 130°C presents little to no mass loss, suggesting the occurrence of a coformer phase transition, likely CL20 transitioning from the ε-polymorph to the γ-polymorph (Turcotte et al. 2005). The peaks at higher heating rates appeared bimodal in nature, rather to the sharper, unimodal peaks observed at lower heating rates.

The TNT/CL20 cocrystal experiences a two-stage decomposition minimum, as shown by its TGA data (Fig. 3.4b). This differs from the TNT/CL20 physical mixture, which clearly experiences a two-stage decomposition (Fig. 3.4d). There is one exception: the data for the cocrystal and the physical mixture corresponding to the 2°C per minute heating rate look alike.

Despite their differences in thermal behavior, the cocrystals ADNP/DAF and TNT/CL20 both have the excellent properties for a melt-castable energetic; primarily, they have lower melting points and similar decomposition temperatures when compared to their physical mixtures and one or both of their coformers (Table 3.3).

Table 3.3. Comparison of Peak DSC temperatures for TNT/CL20 cocrystal, physical mixture, and individual coformers at a 15°C/min heating rate.

Material	Cocrystal	Physical Mixture	TNT	CL20
Peak Endotherm Temp. (°C)	143.4	80.5	81.6	174.2
2nd Endotherm Temp.(°C)	--	135.9	237.7	--
Peak Exotherm Temp.(°C)	256.6	255.9	--	244.3

During hot-stage microscopy of TNT/CL20 cocrystals, several observations were made as shown in Fig. 3.5. Some of the larger particles appeared to have pores internal to their structure (Fig. 3.5a); upon heating, these voids became optically thick and darken (Fig. 3.5b). Also note, the image in Fig. 3.5b is taken at 115°C—well above the melting point of TNT and yet the cocrystals are all intact. As the cocrystal nears the melting onset temperature, these pores appear to expand and fill the interior of the particle (Fig. 3.5c). At 135°C, the cocrystal's outer surface fractures (Fig. 3.5d-e). Prior to the fracture, liquid material is visible within the particle, and the fracture itself is subtle. Immediately after the fracture, the particle resembles a slush mix of liquid material and fractured solid material (Fig. 3.5f-f.1), found to be liquid TNT and β-CL20 by Bolton and Matzger (2011). What is unclear is the mechanism in which this occurs. Two potential mechanisms are apparent. The first potential mechanism is caused when liquid TNT forms inside a CL20 "shell," fractures, and leaves the slush mix of material. The second possible mechanism assumes the particle's composition is a porous structure where the pores are occupied by liquid TNT. This porous structure shatters due to the expansion of the liquid TNT, leaving behind the slush mix of material. Solely based on the evidence contained within this

study, the former seems to be the more probable mechanism; however, a more thorough investigation is required before a confident determination of the mechanism can be made.

At 186°C, the liquid within the sample begins to boil and by 194°C, boiling is widespread across the sample (Fig. 3.5g). By 231°C, the remaining material begins to brown, indicating the decomposition onset of the cocrystal. By 266°C, there is no visible liquid remaining, all residual material has darkened, and the residual material begins to crack as the decomposition progresses to completion.

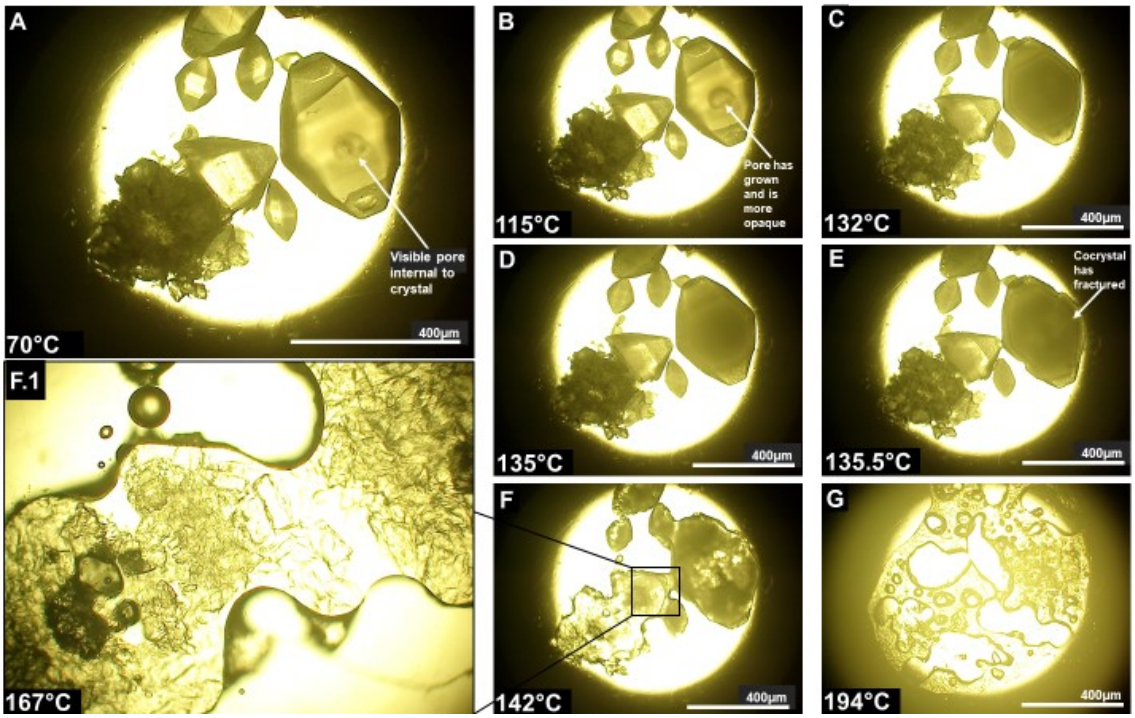

Fig. 3.5. Hot-stage microscopy images of TNT/CL20 cocrystal sample at **a)** 70°C, **b)** 115°C, **c)** 132°C, **d)** 135°C, **e)** 135.5°C, **f)** 142°C, **f.1)** 167°C, and **g)** 194°C.

3.2.3 HMX/CL20

DSC/TGA traces for the HMX/CL20 cocrystal and physical mixture are shown in Fig. 3.6. This cocrystal was unique when compared to the other cocrystals—no endotherms were observed during heating (Fig. 3.6a). Previously, if one or both of the coformers displayed an endotherm, the cocrystal would also display an endotherm. The range of temperatures observed for the peak exothermic temperature was also much narrower than the other cocrystals observed in this study—ranging from 229-243°C—but peak exothermic temperatures do increase with

higher heating rates as expected. Bolton et al. reported the HMX/CL20 cocrystal detonated at approximately 240°C (2012); however, no detonation was observed during these studies. This disparity can be explained due to the different conditions of the DSC experiments: Bolton et al. conducted their experiments using hermetically sealed aluminum pans with a nitrogen purge (2012) while the conditions used in this study involved open alumina pans with an argon purge.

Another more common characteristic of this cocrystal was the broader peaks observed at higher heating rates versus the sharp peaks observed at the lower heating rates. At the higher heating rates, the sample decomposes over a wider range of temperature due to thermal lag. At the lower heating rates, the majority of the sample is at the onset temperature when the cocrystal decomposes; this presents as the exothermic spike observed on the DSC plot (Fig. 3.6a) for the 5°C and 2°C per minute heating rates. The combined behavior across all heating rates suggests the HMX/CL20 cocrystal appears to be more reliant on temperature than on the heating rate.

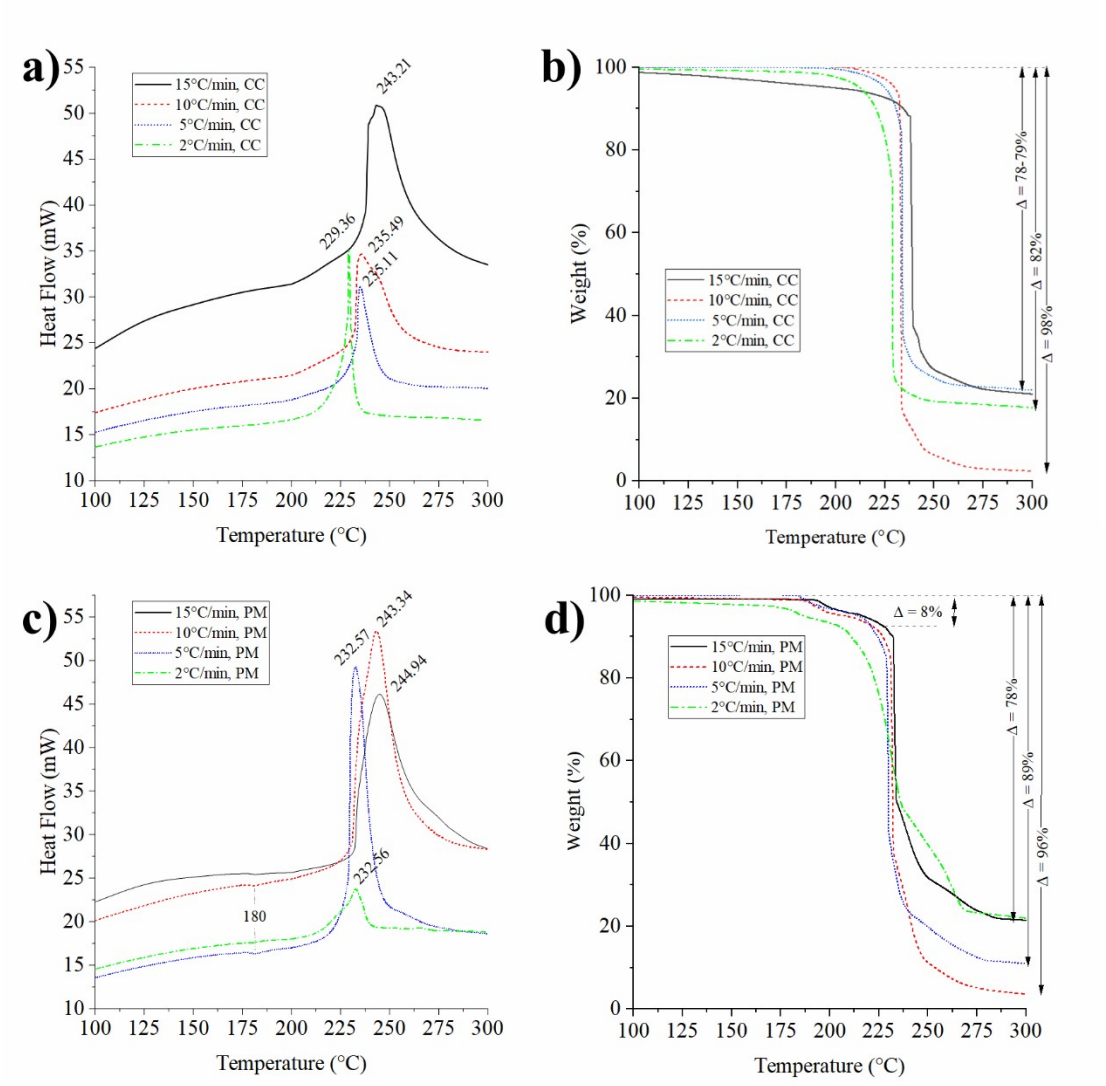

Fig. 3.6. DSC and TGA traces of **(a-b)** HMX/CL20 cocrystal and **(c-d)** HMX/CL20 physical mixture at varying heating rates in open pan. CC and PM as shown in plot legend refer to cocrystal and physical mixture, respectively.

Contrasting the DSC data for the cocrystal and physical mixture provides an interesting observation. An endotherm appears for the physical mixture which is not apparent in the cocrystal, nor does it correlate to the phase transition temperature for CL20 (CL20 transition from ε- to γ- polymorphs takes place at 165°C) (Foltz et al. 1994; Turcotte et al. 2005). This endotherm could be attributed to a solid-solid phase transition of HMX within the physical mixture. The β-HMX to δ-HMX phase transition has been observed at a wide range of temperatures over 159° (Cady and Smith 1962) and corroborates with available literature regarding HMX phase transitions (Fathollahi, Pourmortazavi, and Hosseini 2008).

Similar to TNT/CL20, HMX/CL20 is the second material combination which displays similar exothermic temperatures for both the cocrystal and the physical mixture (see Table 3.4).

Table 3.4. Comparison of Peak DSC temperatures for HMX/CL20 cocrystal, physical mixture, and individual coformers at a 15°C/min heating rate.

Material	Cocrystal	Physical Mixture	HMX*	CL20
Peak Endotherm Temp. (°C)	--	--	187.0	174.2
2nd Endotherm Temp.(°C)	--	--	278.0	--
Peak Exotherm Temp.(°C)	243.2	244.9	280.0	244.4

*(Fathollahi, Pourmortazavi, and Hosseini 2008)

The hot-stage microscopy of the HMX/CL20 cocrystal is captured in Fig. 3.7. Fig. 3.7a is the baseline picture; the yellow tint to the picture results from the Kapton tape used to enclose the sample. To restrict particle movement, the Kapton tape was used to firmly encapsulate the particles; in doing so, some air pockets were created and identified in the picture (Fig. 3.7a). At approximately 220°C, the particles become opaque and appear dark in color; this is noticeable when comparing individual particles at 220°C (Fig. 3.7b) with the same particles at 225°C (Fig. 3.7c). Shortly after this change in appearance, the particles begin producing gaseous products. This is evidenced by the expansion of the air pockets surrounding the particles (Fig. 3.7d). At approximately 248°C, the particles begin to melt (Fig. 3.7e) and boil almost immediately after (Fig. 3.7f). The boiling dissipates at approximately 288°C and leaves a light brown residue. As the decomposition nears its end, the brown residue cracks in a manner similar to the residual material left after the TNT/CL20 decomposition.

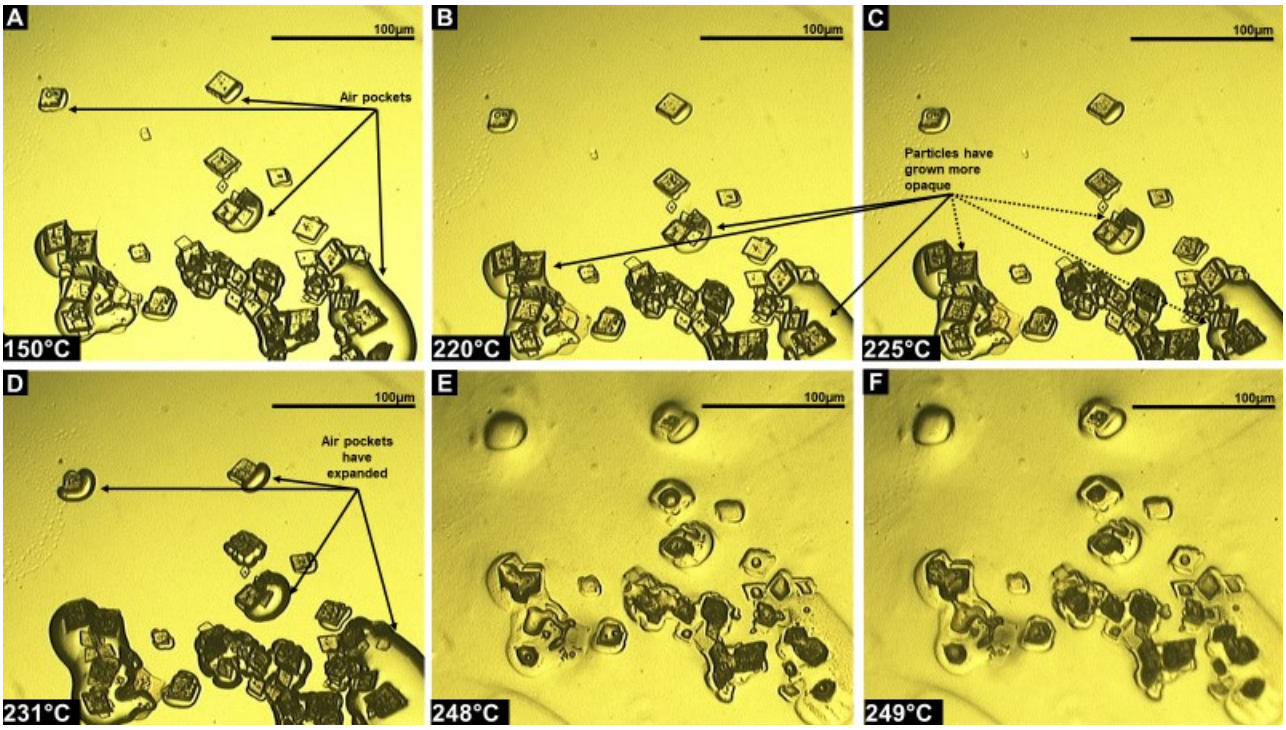

Fig. 3.7. Hot-stage microscopy images of HMX/CL20 cocrystal sample at **a)** 150°C, **b)** 220°C, **c)** 225°C, **d)** 231°C, **e)** 248°C, and **f)** 249°C.

3.2.4 MDNT/CL20

DSC/TGA traces for the MDNT/CL20 cocrystal and physical mixture are shown in Fig. 3.8. The MDNT/CL20 cocrystal experienced an endotherm between 160-170°C and displayed increasing peak exotherm temperatures as heating rates increased, ranging from 230-256°C (Fig. 3.8a). This is another cocrystal which experiences phase stabilization; MDNT's endotherm at 93°C is not apparent in the cocrystal DSC data. The cocrystal TGA data (Fig. 3.8b) corresponding to the endotherm demonstrates a mass loss; this suggests a vaporization process (Banerjee 1993). The overall cocrystal TGA data suggests a two-stage decomposition with very similar behavior across all heating rates. The thermal and kinetics data hints the decomposition of the MDNT/CL20 cocrystal may be more dependent on the heating rate than temperature.

The DSC data from the MDNT/CL20 physical mixture is unique in that it displays two endotherms—one at roughly 93°C and another at between 147-166°C (Fig. 3.8c). The TGA data corresponding to those endotherms suggests melting and evaporation respectively (Fig. 3.8d). The physical mixture also demonstrates a broad range of increasing exotherm temperatures as the heating rates increase, ranging from 228-244°C. The decomposition of the physical mixture

appears to be a two-stage decomposition (Fig. 3.8d); however, there is a clear distinction between the higher heating rates (15°C and 10°C per minute) and the lower heating rates (5°C and 2°C per minute). The higher heating rates appear to experience a greater mass loss over a wider range of temperatures, and the lower heating rates experience less mass loss over a narrower range of temperatures. This finding supports the previous conclusion that the MDNT/CL20 cocrystal decomposition is more reliant on the heating rate than the temperature.

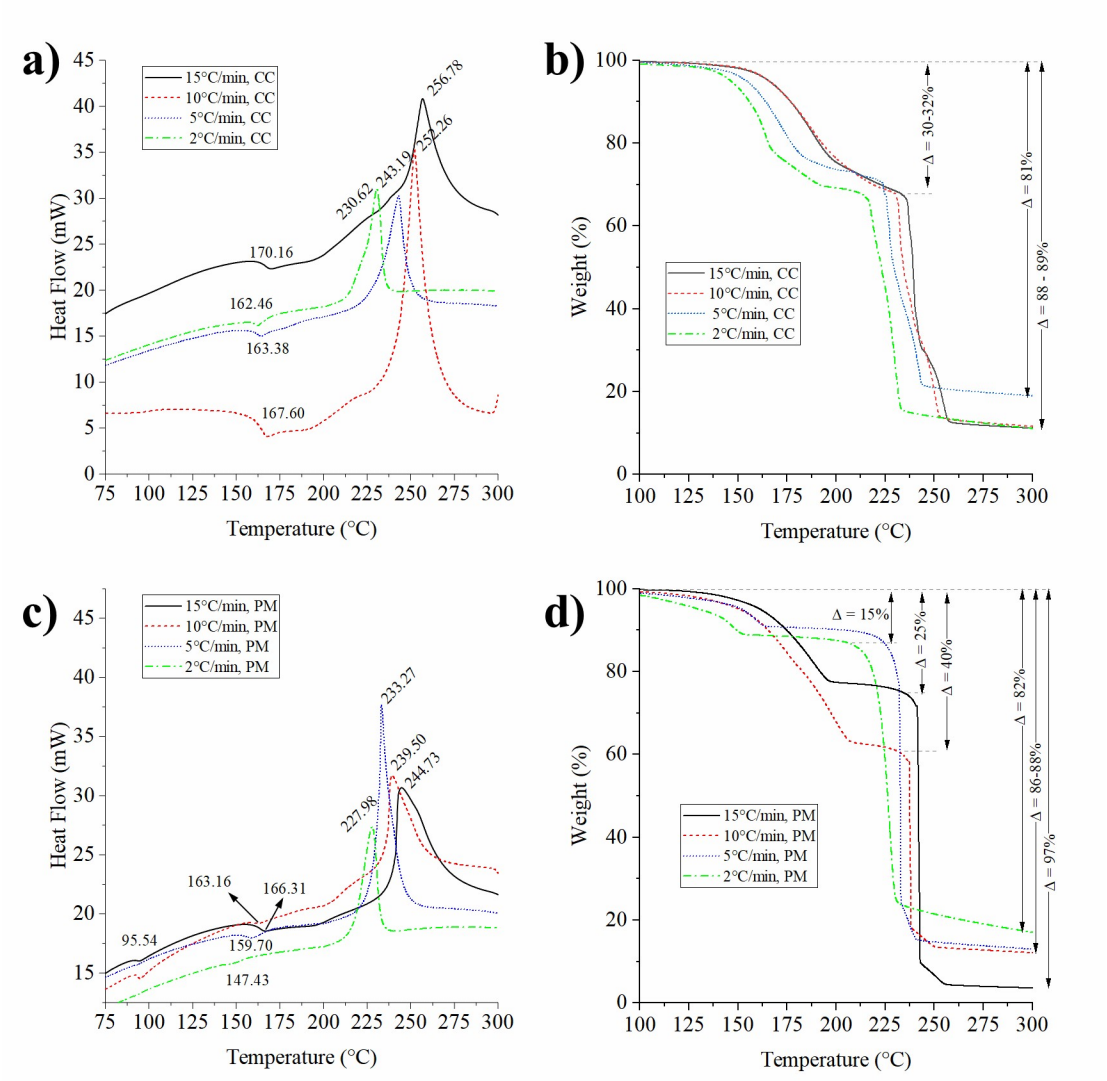

Fig. 3.8. DSC and TGA traces of **(a-b)** MDNT/CL20 cocrystal and **(c-d)** MDNT/CL20 physical mixture at varying heating rates in open pan. CC and PM as shown in plot legend refers to cocrystal and physical mixture, respectively.

The DSC behavior of the MDNT/CL20 cocrystal, physical mixture, and its coformers (Table 3.5) bears a resemblance to the DSC behavior for the ADNP/DAF cocrystal, physical mixture, and its coformers. Both material combinations have a coformer with two endothermic peaks and both cocrystals have higher melting points than their physical mixtures and one or both of their coformers. The significant difference between MDNT/CL20 and ADNP/DAF cocrystals is the MDNT/CL20 cocrystal possesses a higher melting point than its physical mixture. This higher melting point does not support its selection as a potential candidate to replace TNT in a cocrystal melt-castable energetic application.

Table 3.5. Peak DSC Temperature Comparison for MDNT/CL20 Cocrystal, Physical Mixture, and Individual Coformers at a 15°C/Min Heating Rate

Material	Cocrystal	Physical Mixture	MDNT	CL20
Peak Endotherm Temp. (°C)	--	95.5	96.2	--
2nd Endotherm Temp. (°C)	170.2	166.3	218.1	174.2
Peak Exotherm Temp. (°C)	256.8	244.7	--	244.4

Fig. 3.9 captures critical moments observed during the hot-stage microscopy of the MDNT/CL20 cocrystal. Fig. 3.9a is the baseline photo. Some particles melt at 172°C and liquefy by 183°C (Fig. 3.9b). This corroborates with the literature, where MDNT/CL20 was observed through DSC to have a melt/phase transition take place in this range of temperatures (Anderson et al. 2016). Not all of the particles do melt however; some contract in volume and become optically thick (Fig. 3.9c). The combination of the observed partial melt and volume change corroborates our findings from the DSC, where the endotherm and mass loss suggested vaporization was taking place. The aforementioned volume change experienced by the individual particles is significant; in Fig. 3.9d, the original outline of the particles is identified by the red line. By 297°C, all particles darken and major visible changes cease.

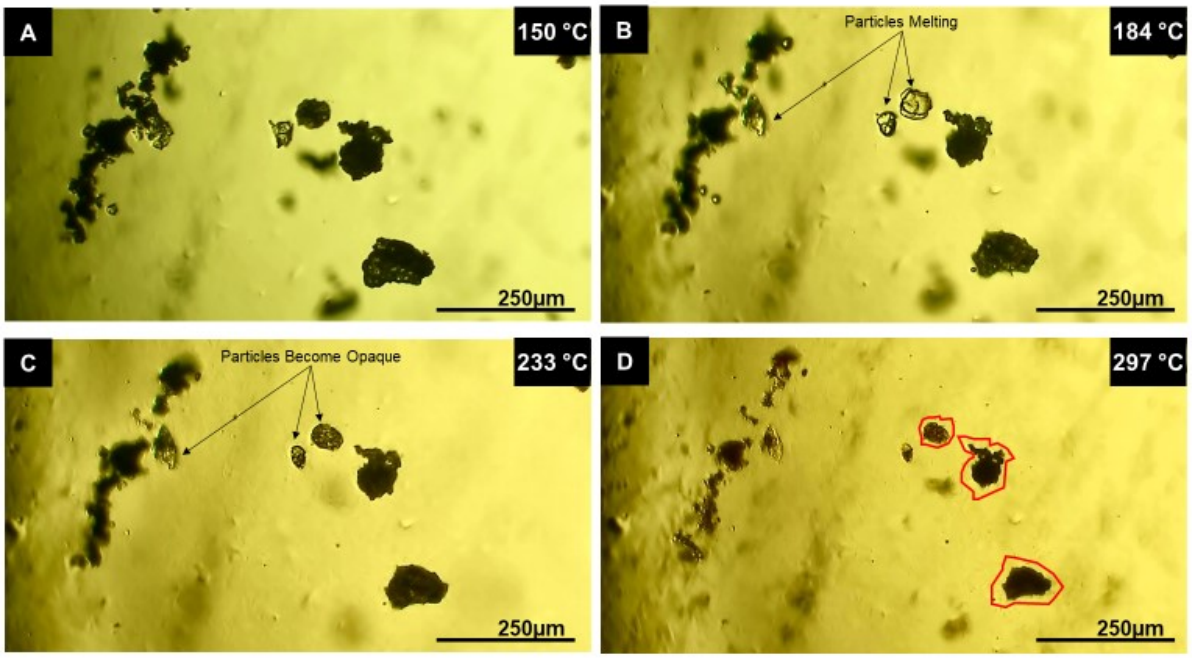

Fig. 3.9. Hot-stage microscopy images of MDNT/CL20 cocrystal sample at **a)** 150°C, **b)** 184°C, **c)** 233°C, and **d)** 297°C.

3.3 Kinetics Analysis

The activation energy and pre-exponential constant produced from the isoconversional Kissinger and Ozawa methods for both the cocrystals and their respective stoichiometric physical mixtures are detailed below in Table 3.6. Included in this table is the r-squared value of the linear trendline applied to the kinetic analysis data. Multiple DSC/TGA runs were required for the HMX/CL20 cocrystal and physical mixtures prior to completion of the kinetics analysis. The Kissinger and Ozawa methods were very sensitive for this coformer combination due to the narrow range of peak exotherm temperatures.

Table 3.6. Isoconversional kinetic parameters for cocrystals and stoichiometric physical mixtures of their coformers.

	Kissinger's Method			Ozawa's Method		
Material	Peak Activation Energy (kJ/mol)	Average ln(A)	R^2	Peak Activation Energy (kJ/mol)	Average ln(A)	R^2
ADNP/DAF	76.75	13.05	0.94	80.71	14.47	0.95
Physical Mixture	87.50	16.63	0.90	90.76	17.75	0.91
TNT/CL20	170.81	34.80	0.99	170.53	34.77	0.99
Physical Mixture	179.18	36.94	0.94	178.48	36.81	0.94
HMX/CL20	308.23	68.63	0.94	301.03	67.41	0.94
Physical Mixture	249.24	54.19	0.90	245.00	53.40	0.90
MDNT/CL20	160.58	32.34	0.99	160.80	32.43	0.99
Physical Mixture	251.36	54.12	0.97	246.99	54.12	0.98

By comparing the kinetic parameters, specifically the activation energy, of the cocrystal and the stoichiometric physical mixture, the ability of cocrystallization to alter thermal decomposition and kinetic behavior becomes clear. ADNP/DAF experiences a 11-13% decrease in activation energy, where TNT/CL20 experiences a smaller decrease of only 5%. HMX/CL20 shows an increase in activation energy, rising by 2%. The HMX/CL20 cocrystal's activation energy found in this study is slightly higher than the literature (Ghosh et al. 2018); however, this disparity can be attributed to the less-than-ideal fit of the linear trendline to the DSC data. MDNT/CL20 is the most remarkable with a staggering decrease of 42-44% in activation energy when the cocrystal is compared against the physical mixture. The variation between the results found using Kissinger's method versus Ozawa's method can be attributed to the different equations used by these methods. Variation in activation energy between the two methods were less than 2%, except in the case of ADNP/DAF where the variation was 5% for the cocrystal and 3% for the physical mixture.

Figure 3.10 shows the activation energy of the cocrystals compared to the activation energies of the physical mixtures and coformers. For the CL20-based cocrystals, it appears the cocrystal activation energy falls between the activation energies of the coformers. For TNT/CL20 and HMX/CL20, there are other cocrystal studies available for comparison. Both studies used for comparison conducted thermal analysis using closed pans versus the open pans in this study. The TNT/CL20 activation energy values found in this study are slightly lower than

those found in the literature, while the reverse is true for the HMX/CL20 cocrystal. This suggests two things. First, closed pans will generally produce lower activation energies than open pans with the same material because the heat and decomposition products are trapped within the closed pan. Second, this suggests the volatility of materials may play a role in lowering the activation energy for the open pan thermal analysis.

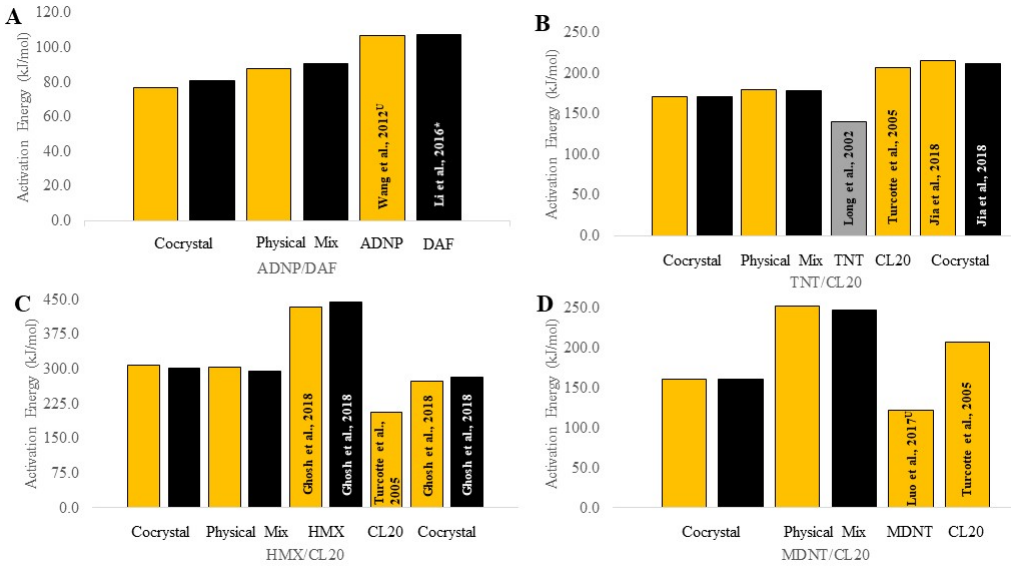

Fig. 3.10. Comparison of the cocrystal, physical mixture, and coformer activation energies for **a)** ADNP/DAF, **b)** TNT/CL20, **c)** HMX/CL20, and **d)** MDNT/CL20.

(Note: Gold indicates the Kissinger method was used for kinetics analysis, black indicates the Ozawa method was used for kinetics analysis, and gray indicates the author did not specify the kinetics analysis method. Also, the asterisk indicates the author used open pans during thermal analysis; the "U" superscript indicates the author did not specify open or closed pans during thermal analysis).

A better assessment of the thermal sensitivity would be the change in peak exotherm temperature. An increase in peak exotherm temperature would make the material less sensitive to temperature and vice versa. The activation energies have more utility as indicators of reaction rate. Materials with lower activation energies react faster than those with higher activation energies. Based on the results above, the ADNP/DAF and MDNT/CL20 cocrystals have faster reaction rates than their physical mixtures. With the remaining two cocrystals, especially TNT/CL20, the reaction rates are marginally faster than their physical mixtures.

In summary, all cocrystals showed different activation energies than their physical mixtures when analyzed using the Kissinger and Ozawa isoconversional kinetics analysis

methods. These results suggest the cocrystallization process could not only alter the performance and sensitivity of its coformers (Bolton and Matzger 2011; Bolton et al. 2012; J. Zhang and Shreeve 2016), but also alter the reaction kinetics. The extent to which cocrystallization affects the reaction kinetics and the mechanisms with which it modifies the thermal behavior remain a mystery; no clear trend emerges from this study as to how cocrystallization affects the reaction kinetics of energetic materials.

4. CONCLUSIONS

We have studied the thermal decomposition of four energetic cocrystals composed of ADNP/DAF, TNT/CL20, HMX/CL20, and MDNT/CL20 and compared to their stoichiometric physical mixtures. The thermal behavior of each cocrystal was also observed and characterized through hot-stage microscopy under conditions which mimicked those used in the DSC/TGA studies. Various decomposition phenomena of the cocrystals were visually observed at temperatures similar to those observed in the DSC/TGA studies. Hot-stage microscopy results corroborated the findings obtained via DSC/TGA.

For ADNP/DAF, the comparison of the cocrystal to the stoichiometric physical mixture shows an 8% increase in the peak exotherm temperature and a 11-13% decrease in peak activation energy. The decomposition of the ADNP/DAF cocrystal consists of the cocrystal melting and then decomposition products vaporizing as temperatures continue to rise. The cocrystal is less thermally sensitive and has a faster reaction rate than its physical mixture. For TNT/CL20, this comparison shows a much smaller change in the peak exotherm temperature (less than 1%) but shows a 5% decrease in activation energy. Through DSC, it is evident the TNT/CL20 cocrystal experiences phase stabilization. Through digital microscopy, the TNT/CL20 cocrystal was observed to melt and fracture into a slush mix of liquid material and crystalline fragments. The TNT/CL20 cocrystal is just as thermally sensitive as its physical mixture but has a faster reaction rate than its physical mixture. For HMX/CL20, this comparison shows less than 1% change in the peak exotherm temperature and shows an 2% increase in activation energy. The HMX/CL20 cocrystal also experiences phase stabilization by displaying no endotherms during the decomposition process. The HMX/CL20 cocrystal and physical mixture demonstrate similar thermal sensitivity; however, the cocrystal may possess slightly slower reaction rates. Finally, for MDNT/CL20, this comparison shows nearly a 4% increase and a staggering 42-44% decrease in peak activation energy. Like TNT/CL20, MDNT/CL20 also experiences phase stabilization as evidenced by the DSC data. Through hot-stage microscopy, a partial melt/phase transition was observed during the MDNT/CL20 cocrystal decomposition. The MDNT/CL20 cocrystal is less thermally sensitive and demonstrates significantly faster reaction rates than its physical mixture.

Based on this study alone, the effects of cocrystallization on its coformers cannot be conclusively stated. However, based on this study alone, cocrystallization shows two potential trends. The first is the majority of the cocrystals in this study saw higher peak exotherm temperatures and decreased thermal sensitivity as a result of the cocrystallization process. The second is all of the CL20 based cocrystals saw phase stabilization of one or both coformers. Cocrystallization clearly exhibits the ability to alter thermal behavior and reaction kinetics of its coformers when compared to stoichiometric physical mixtures or the coformers alone.

REFERENCES

Anderson, Stephen R., Pascal Dubé, Mariusz Krawiec, Jerry S. Salan, David J.am Ende, and Philip Samuels. 2016. "Promising CL-20-Based Energetic Material by Cocrystallization." *Propellants, Explosives, Pyrotechnics* 41 (5): 783–88. https://doi.org/10.1002/prep.201600065.

Banerjee, Debjani. 1993. "Experimental Techniques in Thermal Analysis Thermogravimetry (TG) & Differential Scanning Calorimetry (DSC)." *Analytical Proceedings*, no. 12: 469–508.

Bennion, Jonathan C., Zohaib R. Siddiqi, and Adam J. Matzger. 2017. "A Melt Castable Energetic Cocrystal." *Chemical Communications* 53 (45): 6065–68. https://doi.org/10.1039/c7cc02636f.

Blaine, Roger L., and Homer E. Kissinger. 2012. "Homer Kissinger and the Kissinger Equation." *Thermochimica Acta* 540: 1–6. https://doi.org/10.1016/j.tca.2012.04.008.

Bolton, Onas, and Adam J. Matzger. 2011. "Improved Stability and Smart-Material Functionality Realized in an Energetic Cocrystal." *Angewandte Chemie - International Edition* 50 (38): 8960–63. https://doi.org/10.1002/anie.201104164.

Bolton, Onas, Leah R. Simke, Philip F. Pagoria, and Adam J. Matzger. 2012. "High Power Explosive with Good Sensitivity: A 2:1 Cocrystal of CL-20:HMX." *Crystal Growth and Design* 12 (9): 4311–14. https://doi.org/10.1021/cg3010882.

Cady, H H, and L C Smith. 1962. "Studies on the Polymorphs of HMX." *Los Alamos Scientific Laboratory* LAMS-2652.

Cox, S J. 2005. "USS Forrestal Disaster." US Naval History and Heritage Command. 2005. https://www.history.navy.mil/content/history/nhhc/about-us/leadership/director/directors-corner/h-grams/h-gram-008/h-008-6.html.

Cunningham, J M. 2019. "Texas City Explosion of 1947." In *Encyclopaedia Britannica*. Encyclopaedia Britannica, Inc.

Dickson, P.M., Asay, B.W., Henson, B.F., Smilowitz, L.B. 2004. "Thermal Cook-o Ff Response of Confined PBX 9501." *Royal Society* 460 (August): 3447–55.

Doyle, C. D. 1962. "Estimating Isothermal Life from Thermogravimetric Data." *Journal of Applied Polymer Science* 6 (24): 639–42. https://doi.org/10.1002/app.1962.070062406.

Fathollahi, M., S. M. Pourmortazavi, and S. G. Hosseini. 2008. "Particle Size Effects on Thermal Decomposition of Energetic Material." *Journal of Energetic Materials* 26 (1): 52–69. https://doi.org/10.1080/07370650701719295.

Foltz, M. Frances, Clifford L. Coon, Frank Garcia, and Albert L. Nichols. 1994. “The Thermal Stability of the Polymorphs of Hexanitrohexaazaisowurtzitane, Part I.” *Propellants, Explosives, Pyrotechnics* 19 (1): 19–25. https://doi.org/10.1002/prep.19940190105.

Gao, Bing, Dunju Wang, Juan Zhang, Yingjie Hu, Jinpeng Shen, Jun Wang, Bing Huang, et al. 2014. “Facile, Continuous and Large-Scale Synthesis of CL-20/HMX Nano Co-Crystals with High-Performance by Ultrasonic Spray-Assisted Electrostatic Adsorption Method.” *Journal of Materials Chemistry A* 2 (47): 19969–74. https://doi.org/10.1039/c4ta04979a.

Ghosh, Mrinal, Arun K. Sikder, Shaibal Banerjee, and Rajesh G. Gonnade. 2018. “Studies on CL-20/HMX (2:1) Cocrystal: A New Preparation Method and Structural and Thermokinetic Analysis.” Research-article. *Crystal Growth and Design* 18 (7): 3781–93. https://doi.org/10.1021/acs.cgd.8b00015.

Jia, Qian, Jiaoqiang Zhang, Kaichang Kou, Shijie Zhang, and Yunlong Xu. 2019. “Preparation, Characterization and the Thermodynamic Properties of HNIW · TNT Cocrystal.” *Propellants, Explosives, Pyrotechnics* 44 (5): 588–96. https://doi.org/10.1002/prep.201800330.

Landenberger, Kira B., and Adam J. Matzger. 2010. “Cocrystal Engineering of a Prototype Energetic Material: Supramolecular Chemistry of 2,4,6-Trinitrotoluene.” *Crystal Growth and Design* 10 (12): 5341–47. https://doi.org/10.1021/cg101300n.

Landenberger, Kira B., and Adam J. Matzger. 2012. “Cocrystals of 1,3,5,7-Tetranitro-1,3,5,7-Tetrazacyclooctane (HMX).” *Crystal Growth and Design* 12 (7): 3603–9. https://doi.org/10.1021/cg3004245.

Li, Xi, Qiu han Lin, Xin Ying Zhao, Zhi Wei Han, and Bo liang Wang. 2017. “Compatibility of 2, 4, 6, 8, 10,12-Hexanitrohexaazaisowurtzitane with a Selection of Insensitive Explosives.” *Journal of Energetic Materials* 35 (2): 188–96. https://doi.org/10.1080/07370652.2016.1245372.

Li, Yanfeng, Xiaofeng Wang, Kangzhen Xu, Bozhou Wang, Jirong Song, and Fengqi Zhao. 2016. “Hermetic Thermal Behavior of 3,4-Diaminofurazan (DAF).” *Propellants, Explosives, Pyrotechnics* 41 (5): 888–92. https://doi.org/10.1002/prep.201500330.

Liu, Ke, Gao Zhang, Jieyu Luan, Zhiqun Chen, Pengfei Su, and Yuanjie Shu. 2016. “Crystal Structure, Spectrum Character and Explosive Property of a New Cocrystal CL-20/DNT.” *Journal of Molecular Structure* 1110: 91–96. https://doi.org/10.1016/j.molstruc.2016.01.027.

Rogers, Raymond. 1975. “Thermochemistry of Explosives.” *Thermochimica Acta* 11: 131–39.

Sabatini, Jesse J., and Karl D. Oyler. 2015. “Recent Advances in the Synthesis of High Explosive Materials.” *Crystals* 6 (1): 1–22. https://doi.org/10.3390/cryst6010005.

Schmidt, R D, G S Lee, P F Pagoria, and A R Mitchell. 2001. “Synthesis and Properties of a New Explosive , 4-Amino-3,5-Dinitro-1H-Pyrazole (LLM-116).” *Lawrence Livermore National Laboratory* UCRL-ID-14 (3).

Sis, H. 2009. “Application of Model-Free Methods for Analysis of Combustion Kinetics of Coals with Different Ranks.” *Energy Sources, Part A: Recovery, Utilization and Environmental Effects* 31 (12): 1016–27. https://doi.org/10.1080/15567030802089037.

Turcotte, Richard, Marie Vachon, Queenie S.M. Kwok, Ruiping Wang, and David E.G. Jones. 2005. “Thermal Study of HNIW (CL-20).” *Thermochimica Acta* 433 (1–2): 105–15. https://doi.org/10.1016/j.tca.2005.02.021.

Vuppuluri, Vasant S., Philip J. Samuels, Kelley C. Caflin, I. Emre Gunduz, and Steven F. Son. 2018. “Detonation Performance Characterization of a Novel CL-20 Cocrystal Using Microwave Interferometry.” *Propellants, Explosives, Pyrotechnics* 43 (1): 38–47. https://doi.org/10.1002/prep.201700150.

Wang, Ying Lei, Feng Qi Zhao, Kang Zhen Xu, Yue Ping Ji, Jian Hua Yi, Wei Wang, Tao Yu, and Ting An. 2014. “Synthesis, Thermal Behavior, and Application of 4-Amino-3,5-Dinitropyrazole Lead Salt.” *Journal of Thermal Analysis and Calorimetry* 115 (2): 1219–25. https://doi.org/10.1007/s10973-013-3457-9.

Yang, Zongwei, Hongzhen Li, Xiaoqing Zhou, Chaoyang Zhang, Hui Huang, Jinshan Li, and Fude Nie. 2012. “Characterization and Properties of a Novel Energetic-Energetic Cocrystal Explosive Composed of HNIW and BTF.” *Crystal Growth and Design* 12 (11): 5155–58. https://doi.org/10.1021/cg300955q.

Zhang, Jiaheng, and Jean’Ne M. Shreeve. 2016. “Time for Pairing: Cocrystals as Advanced Energetic Materials.” *CrystEngComm* 18 (33): 6124–33. https://doi.org/10.1039/c6ce01239f.

Zhang, Jiao Qiang, Yun Long Xu, Qian Jia, Shi Jie Zhang, Ning Liu, Hong Xu Gao, and Rong Zu Hu. 2018. “Nonisothermal Decomposition and Safety Parameters of HNIW/TNT Cocrystal.” *RSC Advances* 8 (54): 31028–36. https://doi.org/10.1039/C8RA06143B.

Zhu, Yan Li, Ming Xin Shan, Zhi Xia Xiao, Jing Si Wang, and Qing Jie Jiao. 2015. “Kinetics of Thermal Decomposition of ε-Hexanitrohexaazaisowurtzitane by TG-DSC-MS-FTIR.” *Korean Journal of Chemical Engineering* 32 (6): 1164–69. https://doi.org/10.1007/s11814-014-0305-y.